



Optics Letters

High-precision 3D surface topography measurement using high-stable multi-wavelength digital holography referenced by an optical frequency comb

DAHI GHAREAB ABDELSALAM IBRAHIM^{1,2,3,*} AND TAKESHI YASUI^{2,3}

¹Engineering and Surface Metrology Laboratory, National Institute of Standards, Tersa St., El haram, El Giza, Egypt

²Graduate School of Technology, Industrial and Social Sciences, Tokushima University, 2-1, Minami-Josanjima, Tokushima 770-8506, Japan

³JST, ERATO, MINOSHIMA Intelligent Optical Synthesizer Project, 2-1, Minami-Josanjima, Tokushima 770-8506, Japan

*Corresponding author: dahi.abdelsalam@nis.sci.eg

Received 11 December 2017; revised 14 February 2018; accepted 12 March 2018; posted 16 March 2018 (Doc. ID 315397); published 10 April 2018

High-stable, two-wavelength, digital holography referenced by an optical frequency comb is presented. The technique is demonstrated by using optical waves from an external cavity laser diode phase-locked to a mode-locked Er-doped fiber comb laser light. The mixed beat signal is stabilized at 30 MHz by a sensitive proportional integral derivative controller. The tunable continuous-waves stabilized with frequency uncertainty of 5×10^{-11} are employed to investigate large stepped structures. © 2018 Optical Society of America

OCIS codes: (120.3180) Interferometry; (090.1995) Digital holography; (120.6660) Surface measurements, roughness; (180.6900) Three-dimensional microscopy; (120.0120) Instrumentation, measurement, and metrology.

<https://doi.org/10.1364/OL.43.001758>

The main advantage of digital holography (DH) is that it makes it possible to extract quantitatively the three-dimensional (3D) information of the phase object from the numerical reconstruction of a single digitally recorded hologram [1–3]. In general, a hologram refers to the interference pattern between the light scattered by a 3D object and a mutually coherent reference beam. The amplitude and phase information are encoded in the fringe structure of the hologram and can be recovered and used for many applications. Different approaches were used to retrieve the phase object based on a single wavelength. However, a serious limitation to their use is that they can only handle smooth profiles and step heights less than half a wavelength. One of the approaches adapted to overcome the problem of a small dynamic range is based on two-wavelength interferometry [4]. In the two-wavelength method, a careful choice of wavelengths enables the system to make use of long-range measurements. If the phase of the object is measured at two wavelengths, λ_1 and λ_2 , then the synthetic beat wavelength $\lambda_{\text{beat}} = \lambda_1 \lambda_2 / |\lambda_1 - \lambda_2|$. Because of the normal instability of

the two-wavelengths used, the synthetic beat wavelength is fluctuated and, hence, an inherent phase error is produced. Since the ambiguity range characterizes the measurement range, this fluctuation limits the measurement range (can be achieved with at least $\lambda_1 - \lambda_2 = 1.00$ nm or more). In this Letter, we increased the measurement range ($\lambda_1 - \lambda_2 = 0.08$ pm) and minimized the inherent phase error to zero by using high-stable two-wavelength DH configuration referenced to one of the optical frequency comb (OFC) lines of a commercial fiber comb laser (FC1500-250-WG, Menlo Systems GmbH, Munich, Germany), which is phase-locked to a rubidium (Rb) atomic clock (FS725, Stanford Research Systems, accuracy = 5×10^{-11} and instability = 2×10^{-11} at 1 s). The merits of using an OFC include improvement of wavelength stability, reduction of laser line width, and the ability to generate two-wavelength light with arbitrary wavelength difference ($0.08 \text{ pm} < \lambda_1 - \lambda_2 < 70 \text{ nm}$). This technique makes it possible to feature stepped structures as large as 10 m depth with per minute-order resolution. To the best of our knowledge, this is the first attempt on high precision, wide dynamic range measurement using high-stable two-wavelength DH based on OFC lines of a mode-locked fiber comb laser.

In this Letter, two wavelengths $\lambda_1 = 1542.7661$ nm and $\lambda_2 = 1534.8211$ nm, yielding a synthetic beat wavelength $\lambda_{\text{beat}} = 298 \mu\text{m}$, are used in a series. Using these high-stable two wavelength signals, a beat wavelength is synthesized and allowed to measure a rough surface of a Japanese 1-yen coin. For each high-stable wavelength, a single-shot off-axis hologram is captured by a cooled InGaAs CCD camera (Goldeye P-008, Allied Vision Technologies GmbH, 320×256 pixels, pixel size = $30.0 \mu\text{m}$). The intensity distribution in the off-axis hologram formed by the interference of both object and reference beams can be formulated to Eq. (1) [2]:

$$I(k, l) = |O|^2 + |R|^2 + R^*O + RO^*, \quad (1)$$

where O is the object beam, R is the reference beam, $*$ denotes the complex conjugate, and k, l are discrete coordinates in the

hologram plane. In Eq. (1), the first two intensity terms are of zero order, which can be directly filtered in the Fourier domain [5,6], and the last two are the interference terms which include the interference phase. The single-wavelength phase is computed individually by the angular spectrum method [7]. Then, by subtracting the phase image of one wavelength from the phase image of the second image, an equivalent phase image is expressed by Eq. (2):

$$\varphi_{\text{beat}} = \varphi(\lambda_2) - \varphi(\lambda_1). \quad (2)$$

The equivalent phase image is synthesized which allows for imaging much larger axial ranges. By measuring the accurate values of both the synthesized phase and the equivalent wavelength, the optical path difference Δz is calculated precisely according to Eq. (3):

$$\varphi_{\text{beat}} = 4\pi\Delta z(\lambda_1 - \lambda_2)/\lambda_1\lambda_2 = 4\pi\Delta z/\lambda_{\text{beat}}. \quad (3)$$

From Eq. (3), it is evident that by measuring the interference phase and knowing the synthetic beat wavelength, the optical path difference is obtainable. In addition, Eq. (3) shows that any small change in the synthetic beat wavelength produces an error in the optical path difference, so it was essential to stabilize the wavelengths to one of the OFC lines of the fiber comb laser. The optical frequencies, ν_n , of the comb lines can be formulated to Eq. (4) [8]:

$$\nu_n = f_{\text{ceo}} + n f_{\text{rep}} + f_{\text{beat}}, \quad (4)$$

where n is an index the comb line, f_{rep} is the repetition frequency, f_{ceo} is the carrier envelope offset frequency, and f_{beat} is the beat frequency. A representation of the output field of a mode-locked fiber comb laser in frequency domain, including the definition of the f_{ceo} , f_{rep} , and f_{beat} , is shown in Fig. 1.

Frequencies f_{rep} and f_{ceo} , respectively, were locked at 250 and 20 MHz, whereas f_{beat} was stabilized at $f_{\text{beat}} = 30$ MHz by the proportional integral derivative (PID) controller.

Our system is presented in Fig. 3. The system is composed of two sources. The first source emits tunable continuous-wave (CW) light in the range of (1520–1590 nm) by an external cavity laser diode (ECLD). The second is a mode-locked Er-doped fiber comb laser light (center wavelength $\lambda_c = 1550$ nm, spectral band width $\Delta\lambda = 73$ nm, pulse duration $\Delta\tau = 100$ fs, and mean power $P_{\text{mean}} = 380$ mW). Two rotatable $\lambda/2$ -wave plates and a polarized beam splitter serve for setting polarization direction, as well as the power, of the two different beams. The beams diffracted from a diffraction grating are mixed to generate a beat signal. This beat signal is detected by a high-speed photodetector (Thorlabs, InGaAs amplified detector, 700–1800 nm) and monitored by a radio frequency (RF) spectrum analyzer, as shown in Fig. 2(a). The

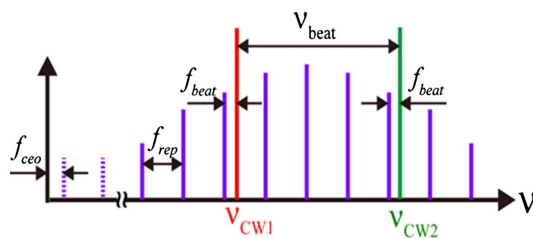


Fig. 1. Representation of the output field of a mode-locked fiber comb laser in frequency domain, including the definition of the f_{ceo} , f_{rep} , and f_{beat} .

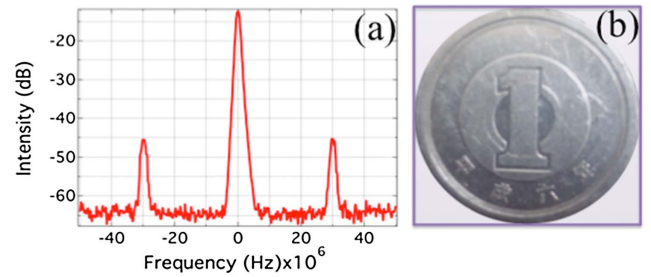


Fig. 2. (a) Beat signal stabilized by PID at $f_{\text{beat}} = 30$ MHz, as seen by an RF spectrum analyzer, and (b) a photograph of the investigated rough Japanese 1-yen coin sample.

free-running beat signal is stabilized at 30 MHz by the PID controller. The n value in Eq. (4) was determined by a wavelength meter (AQ6151, Yokogawa Test & Measurement Corporation, wavelength accuracy = 0.3 pm). The optical frequencies ν_{CW1} and ν_{CW2} were adjusted in a series by changing n and/or f_{rep} . A representation of these frequencies ν_{CW1} and ν_{CW2} which gives the beat signal ν_{beat} is schematically shown in Fig. 1. This synthetic beat frequency is related to the synthetic beat wavelength λ_{beat} , according to Eq. (5):

$$\nu_{\text{beat}} = \nu_{\text{CW2}} - \nu_{\text{CW1}} = c/\lambda_{\text{beat}}, \quad (5)$$

where c is the speed of light. Based on Eqs. (4) and (5), λ_1 , λ_2 , and λ_{beat} were determined.

Two wavelengths of $\lambda_1 = 1542.7661$ nm and $\lambda_2 = 1534.8211$ nm with a power of 2.5 mW were used in a series to feed into a Michelson-type interferometer. The coin sample was placed at one arm of the interferometer, while the other arm was referenced by a gold mirror (suitable for near-infrared light) of flatness $\lambda/10$. After reflecting from the sample and reference mirror, the two beams are recombined at the nonpolarizing beam splitters (NPBS). The interfering object beam (O) and the reference beam (R) were tilted at a small angle with respect to each other to produce an off-axis hologram and to be

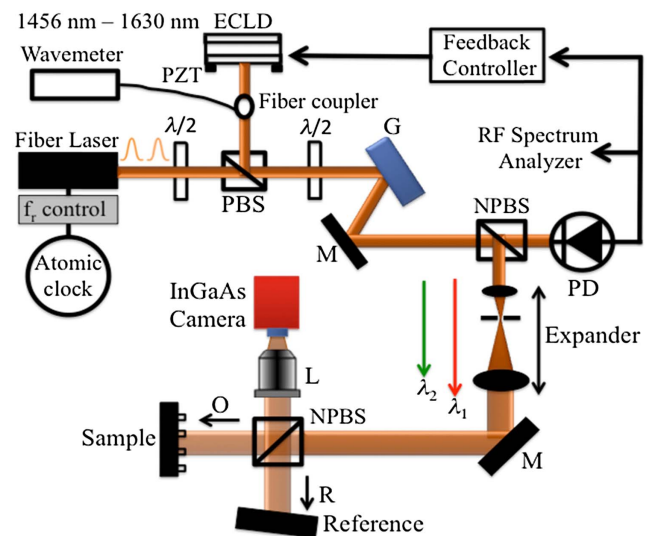


Fig. 3. Experimental setup. ECLD, external cavity laser diode; PZT, piezoelectric transducer; G, grating; M, mirror; PBS, polarizing beam splitter; NPBS, nonpolarizing beam splitters; PD, photodetector.

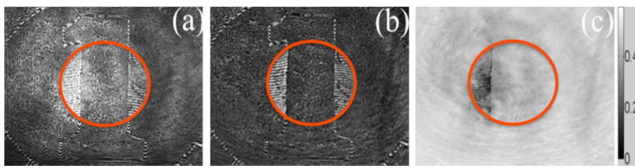


Fig. 4. (a) Original off-axis hologram at a wavelength 1542.7661 nm, (b) correction of (a), and (c) the difference between (a) and (b).

transferred via an imaging lens L ($NA = 0.4$) to the cooled IR InGaAs camera.

To minimize the background noise produced by the ambient medium, a single-shot off-axis hologram is captured at each wavelength. The captured off-axis holograms were corrected by a flat fielding method to reduce the speckle noise [9–11]. The corrected off-axis holograms were further corrected by using 4×4 median filters. Figure 4(a) shows the off-axis hologram captured at $\lambda_1 = 1542.7661$ nm. Figure 4(b) shows the corrected off-axis hologram of Fig. 4(a) by using both a flat fielding method and a 4×4 median filter. The intensity and phase of the corrected off-axis hologram was numerically retrieved by using the angular spectrum method. Figures 5(a)–5(c) show the 3D pseudo-color reconstructed amplitude-contrast images of the red circles of Fig. 4. Figures 5(d)–5(f) show the corresponding 3D pseudo-color reconstructed phase-contrast images. It is worth mentioning that using flat fielding in reconstruction of scattering objects is preferable; otherwise, the structure of the object is partially lost, as shown in Fig. 5.

Figure 6(a) shows the 3D pseudo-color reconstructed phase difference (reversed direction of the x -axis) map of two off-axis holograms captured at wavelengths $\lambda_1 = 1542.7661$ nm and $\lambda_2 = 1534.8211$ nm.

To measure clearly the depth of the pattern one (number 1) on the front face of the Japanese coin, a grafting process has been done. In this process, the phases of an array of pixels (125×195) along the x -axis and (5×150) along the y -axis are converted to maximum phases. Cut lines before and after grafting along the red and blue lines in the phase-contrast images of Figs. 6(a) and 6(b), respectively, are shown in Fig. 6(c), indicating the cross-sectional profile of 164 pixels. Based on Fig. 6(c), the step height is calculated to be $139.9995 \mu\text{m}$,

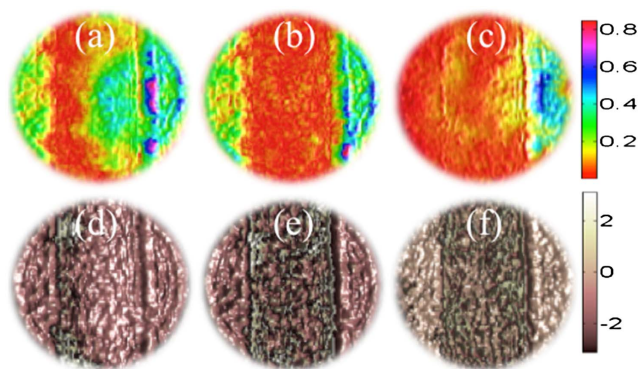


Fig. 5. 3D pseudo-color reconstructed amplitude-contrast image of a single wavelength of (a) Fig. 4(a), (b) Fig. 4(b), (c) Fig. 4(c), and (d) the corresponding phase-contrast images.

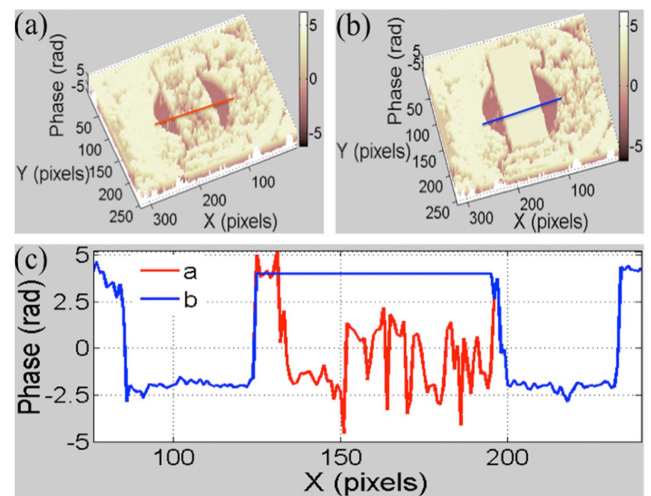


Fig. 6. (a) 3D pseudo-color synthesized phase of two off-axis holograms captured at the two wavelengths $\lambda_1 = 1542.7661$ nm and $\lambda_2 = 1534.8211$ nm, (b) grafting of (a), and (c) 1D phase profiles along both the red and blue lines of (a) and (b).

which matches very well with the nominal value measured with the confocal microscope. In Fig. 6, the 3D reconstructed phase maps were flipped upside down to see the surface from a different side [12]. An experiment on another step height object was performed to demonstrate the effectiveness of our approach. A representation of the step sample of surface height of around 7.00 mm measured roughly by a digital micrometer is shown in Fig. 7(a). The sample was tested by two super-stable wavelengths at $\lambda_1 = 1540.4010$ nm and $\lambda_2 = 1541.4015$ nm. The captured off-axis holograms at each wavelength were corrected by a flat fielding method to reduce the speckle noise and then were numerically reconstructed by using the angular spectrum method.

The retrieved phase maps of the two wavelengths are then subtracted, and a 1D phase profile along the X -axis is shown in Fig. 7(b). The phase is then converted to height and, as seen in Fig. 7(b), the step height is in the range of 7.1800 mm.

In conclusion, we have presented a new method utilizing high-stable, two-wavelength, DH referenced by an OFC. The merits of using an OFC are high accuracy, high stability, and large range ambiguity which, as whole, are unavailable in existing approaches, which makes it adequate for metrology applications. The presented method was effectively applied

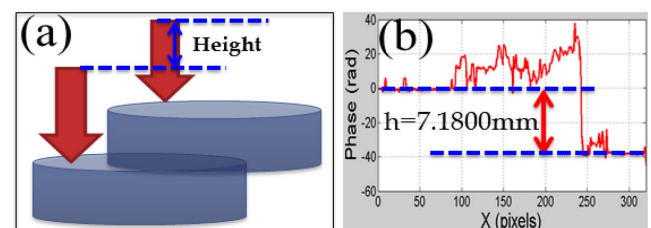


Fig. 7. (a) Representation of the step sample of a 7.00 mm step height measured at super-stable two wavelengths $\lambda_1 = 1542.7661$ nm and $\lambda_2 = 1534.8211$ nm. (b) 1D phase profile along the X -axis of the reconstructed phase difference.

for testing two different stepped structures of 140 μm and 7.00 mm, and the results showed excellent matching with the nominal values. We claim that this method can be used for stepped structures as large as 10 m depth with high precision, and this will be the next step of our research work. The high precision is mainly due to the high stability of wavelengths that are referenced by an OFC lines of a fiber comb laser, which is stabilized to the (Rb) atomic clock with frequency uncertainty of 5×10^{-11} .

Funding. Ministry of Education, Culture, Sports, Science and Technology (MEXT) (26246031); Exploratory Research for Advanced Technology (ERATO); Japanese Science and Technology Agency (MINOSHIMA Intelligent Optical Synthesizer Project, JPMJER1304); Mitutoyo Association for Science and Technology (MAST).

REFERENCES

1. M. Born and E. Wolf, *Principles of Optics* (Cambridge University, 1980).
2. D. G. Abdelsalam and D. Kim, *Appl. Opt.* **50**, 6153 (2011).
3. M. K. Kim, *Digital Holographic Microscopy, Principles, Techniques, and Applications* (Springer, 2011).
4. Y.-Y. Cheng and J. C. Wyant, *Appl. Opt.* **23**, 4539 (1984).
5. E. Cucho, P. Marquet, and C. Depeursinge, *Appl. Opt.* **39**, 4070 (2000).
6. E. Cucho, F. Bevilacqua, and C. Depeursinge, *Opt. Lett.* **24**, 291 (1999).
7. J. Weng, J. Zhong, and C. Hu, *Opt. Express* **16**, 21971 (2008).
8. J. Ye and S. T. Cundiff, *Femtosecond Optical Frequency Comb: Principle, Operation and Applications* (Springer Science + Business Media, 2005).
9. D. G. Abdelsalam and D. Kim, *Opt. Express* **19**, 17951 (2011).
10. D. G. Abdelsalam, M. S. Shaalan, and M. M. Elokher, *Opt. Lasers Eng.* **48**, 543 (2010).
11. D. G. Abdelsalam, M. S. Shaalan, M. M. Elokher, and D. Kim, *Opt. Lasers Eng.* **48**, 643 (2010).
12. D. G. Abdelsalam and T. Yasui, *Appl. Opt.* **56**, F1 (2017).